RSC Advances

PAPER

Cite this: *RSC Adv.*, 2015, **5**, 31472

Nanoscale architecture of bimetallic hybrid Fe–Au nanostructures with and without 1,4-phenylene diisocyanide pre-functionalization†

Youngku Sohn,[ab] Debabrata Pradhan,[ac] Jung-Soo Kang[a] and K. T. Leung*[a]

The nanoscale architecture of a hybrid material has been very important in deriving a new interesting synergic property. Here, we have demonstrated that the functionalization of Au by 1,4-phenylene diisocyanide (PDI) provides a new platform of fabricating smart hybrid materials by electrochemistry. Iron nanorice particles (Fe NrPs) have been electrochemically hybridized with bare and PDI-functionalized Au nanoisland (NI) templates. Their interfacial electronic structures and morphologies have been studied and compared with those of Au sputter- or electro-deposited on Fe NrPs without PDI pre-functionalization. The electrochemically prepared Fe NrP is found to consist of an Fe–FeO core–shell structure covered by thin Fe_2O_3 and/or FeOOH by using depth-profiling X-ray photoelectron spectroscopy (XPS). Remarkably, bare Au NIs supported on Si become aggregated to form bigger islands upon applying a potential. PDI functionalization of Au prevents such a potential-induced aggregation, thereby facilitating Fe NrPs to be deposited on top of the Au NI templates without translocating the Au NIs. No notable difference in the XPS features between Fe on Au with and without PDI-functionalization are found, with no evidence of interfacial Au–Fe alloy formation. For Au on Fe NrPs, the Au 4f XPS peak is shifted to a higher binding energy position with sputtering depth, suggesting the formation of cationic Au–O chemical bonding species at the interface.

Received 10th February 2015
Accepted 24th March 2015

DOI: 10.1039/c5ra02564h

www.rsc.org/advances

1. Introduction

Hybrid nanoscale architectures have attracted a lot of recent attention in various research and industrial fields including energy, catalysis, solar cells, and fuel cells.[1–6] To develop (or enhance) the role of a functional material for a targeted application, architectural processes to control, *e.g.*, the size and shape of a nanoparticle have been developed.[7–10] Two different elements have also been joined together or hybridized to construct various different types of nanostructures such as core–shell and alloy in order to produce the desirable synergetic effects.[11–14] Nanoparticles (NPs) have been supported on transition metal oxides to generate different properties from those of unsupported NPs. For example, Au NPs supported on metal oxides have been found to exhibit enhanced catalytic activities.[15–19] Au is a promising catalyst (*e.g.*, low-temperature CO oxidation) and a sensor material (*e.g.*, surface plasmon and surface-enhanced Raman scattering) when the size decreases to the nanometer regime.[20–22] Fe and Fe oxides have been widely used as magnetic materials (*e.g.*, magnetic resonance imaging and magnetic tape), catalysts, sensors, and drug delivery.[23–26] Hybridization of Au and Fe is therefore expected to provide a synergic effect in the aforementioned applications. It has extensively been reported that Fe oxides and Au NP could be combined to act as a catalyst for low-temperature CO oxidation or water gas shift ($CO + H_2O \rightarrow CO_2 + H_2$) reaction.[16–18,27–32] For application as a sensor, Gu *et al.* have shown that poly-(ethylenimine) functionalized graphene/Fe_3O_4 hybrids assembled with luminol-Au NPs can be used as a platform for the determination of HeLa cells.[33] Furthermore, Bao *et al.* have demonstrated that Au–Fe_3O_4 NPs could be used for protein separation using the magnetic property of Fe_3O_4 and self-assembly property of Au *via* Au–S bonding.[34] It has been demonstrated that near-IR absorption of Au–Fe_3O_4 can be utilized for potential applications as a photothermal treatment of cancer and a drug delivery system.[35–37] For a Fe oxide/Au core–shell structure, the Au shell thickness has been manipulated to tune their plasmonic properties.[38,39]

[a]*WATLab and Department of Chemistry, University of Waterloo, Waterloo, Ontario N2L 3G1, Canada. E-mail: tong@uwaterloo.ca*

[b]*Department of Chemistry, Yeungnam University, Gyeongsan, Gyeongbuk 712-749, South Korea*

[c]*Materials Science Center, Indian Institute of Technology, Kharagpur, West Bengal 721 302, India*

† Electronic supplementary information (ESI) available: *I–t* curves of bare and PDI-functionalized Au NI templates, and Fe electrodeposition on bare Si, bare Au NI template, and PDI-functionalized Au NI template. SEM images of Fe NrPs electrodeposited on PDI-functionalized Au NIs. Cyclic voltammograms. XPS spectra of Fe 2p, O 1s, Au 4f and valence band (VB) regions of Fe electrodeposited on large Au NIs. Review of Au 4f XPS of Fe–Au hybrid materials. See DOI: 10.1039/c5ra02564h

Various methods of synthesizing Fe oxides have been reported.[26] Our group has previously showed that oval-shape (or rice) Fe–Fe oxides core–shell NPs could be prepared on H-terminated Si(100) substrate by a facile electrodeposition method.[40,41] The present work shows that Fe–Fe oxides core–shell NPs could be electrodeposited not just on Si but also on a Au nanoisland (NI) template supported on Si. Furthermore, the effect of Au functionalization by an organic molecule, particularly 1,4-phenylene diisocyanide (PDI, $^{-}C{\equiv}N^{+}{-}C_6H_4{-}N^{+}{\equiv}C^{-}$), and the novel properties of the resulting hybrid nanosystems are illustrated. Since PDI has two parallel isocyanide groups, PDI can act as a linker molecule between two different metal electrodes (or metal nanoparticles). The bonding between the functional group and the metal surface can be understood in terms of σ- and π-bonding.[42–46] PDI is found to have the tendency to self-assemble with gold to form –(Au–PDI)$_n$– oligomers.[42,43] PDI functionalization therefore introduces a significant effect on the electrochemical nanoscale architecture of Au–Fe hybridized nanostructures on a Si substrate.

2. Experimental section

A thin Au film on a Si(100) substrate was prepared by sputter-deposition using a magnetron sputter-coater (Denton Desk II). An Au NI template was prepared by annealing the Au film on the Si substrate at a desired temperature for 1 hour in a muffle oven. The size of the Au NIs could be controlled by adjusting the sputter deposition time and annealing temperature, described in detail elsewhere.[47] Fe was electrodeposited on an Au NI template or a bare Si substrate potentiostatically by amperometry in a three-electrode cell with a CH Instruments 660A electrochemical workstation. A standard Ag/AgCl electrode and a platinum wire were used as the reference and counter electrodes, respectively. The working electrode was a single-side-polished rectangular (15 × 2.5 mm^2) Si(100) chip (0.4 mm-thick, p type with a resistivity of 1.0–1.5 mΩ cm). For Fe electrodeposition, the concentration of deoxygenated aqueous solution of $FeCl_3$ was fixed at 10 mM, and a 100 mM of $NaClO_4$ solution was used as a supporting electrolyte.[40,41] Upon electrodeposition, the samples were thoroughly rinsed with Millipore water (18.2 MΩ cm resistivity), and dried under nitrogen gas stream before scanning electron microscopy (SEM) and X-ray photoelectron spectroscopy (XPS) analyses. The Fe deposition was also performed on a PDI-functionalized Au NI template. For PDI functionalization, a bare Au NI template was immersed in a 1 mM 1,4-phenylene diisocyanide toluene solution for 12 hours, and then fully rinsed with fresh toluene several times to remove multilayer PDI. The surface morphology was examined by field-emission SEM in a LEO 1530 microscope. The chemical states of the samples were analyzed by XPS as a function of Ar^+ ion sputtering time, using a Thermo-VG Scientific ESCALab 250 microprobe with a monochromatic Al Kα X-ray source (1486.6 eV) and a typical energy resolution of 0.4–0.5 eV at full width at half maximum (fwhm). For Ar^+ ion sputtering, an ion beam energy of 3 keV and an ion current density of 0.1–0.2 μA mm^{-2} were employed.[41]

3. Results and discussion

Fig. 1 shows the SEM images of templates of bare Au NIs (Sample A), each with size <10 nm, and of oval-shaped Fe nanorice particles (NrPs) of 100–500 nm in length and 15–100 nm in width electrodeposited on either PDI-functionalized (Sample B) or bare Au NI templates (Sample C). The Au NI template shows no discernible difference in morphology before (Fig. 1, Sample A) and after PDI functionalization (Fig. 1, Sample A1). Remarkably, upon Fe deposition at an applied voltage of −1.0 V the Au NIs functionalized by PDI appear to remain intact (Fig. 1, Sample B) while the bare Au NIs are critically disturbed (Fig. 1, Sample C). As clearly seen at a higher magnification image (Fig. 1, Sample C, inset), the bare Au NIs appear to have relocated from their original positions, resulting in uneven separations among NIs, in order to be hybridized with Fe NrPs. Furthermore, Au NIs are found to cluster on the individual Fe NrPs, and become aggregated, forming bigger Au islands, on the Si support. Consequently, the number density of the Au NIs has drastically decreased.

In order to understand the effect of applied voltage on the rearrangement of Au NIs, we examine the PDI-functionalized (Sample A1) and bare (Sample A2) Au NI templates upon applying a voltage of −3.0 V for 10 min in a blank deionized water solution, *i.e.* without any electrolyte (the corresponding current–time curves shown in ESI, Fig. S1†). Evidently, no discernible change in the morphology is observed for the

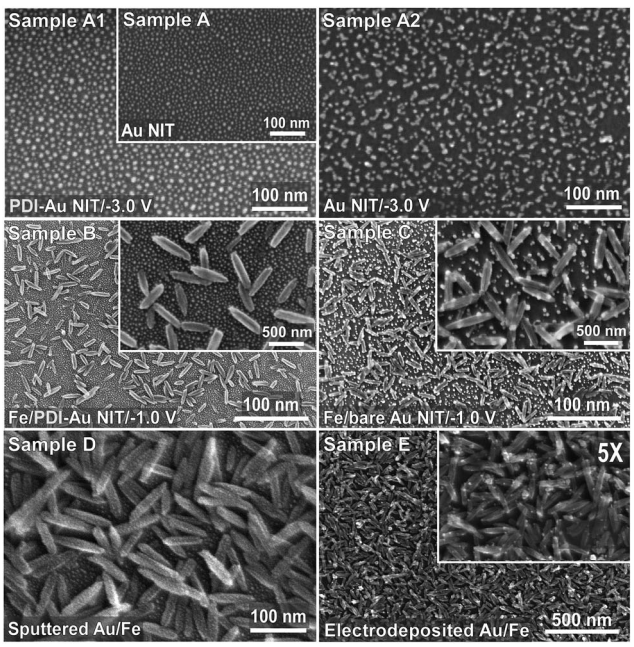

Fig. 1 SEM images of bare Au nanoisland template (NIT, Sample A), and upon applying −3.0 V for 10 min to Au NIT with (Sample A1) and without PDI functionalization (Sample A2); of Fe nanorice particles (NrPs) electrodeposited at −1.0 V for 120 s on Au NIT with (Sample B, inset; magnified scale) and without PDI-functionalization (Sample C, inset; magnified scale); and of Au nanoparticles obtained on both Fe NrPs and the Si substrate by magnetron sputtering (Sample D) and electrodeposition at −1.0 V for 300 s (Sample E).

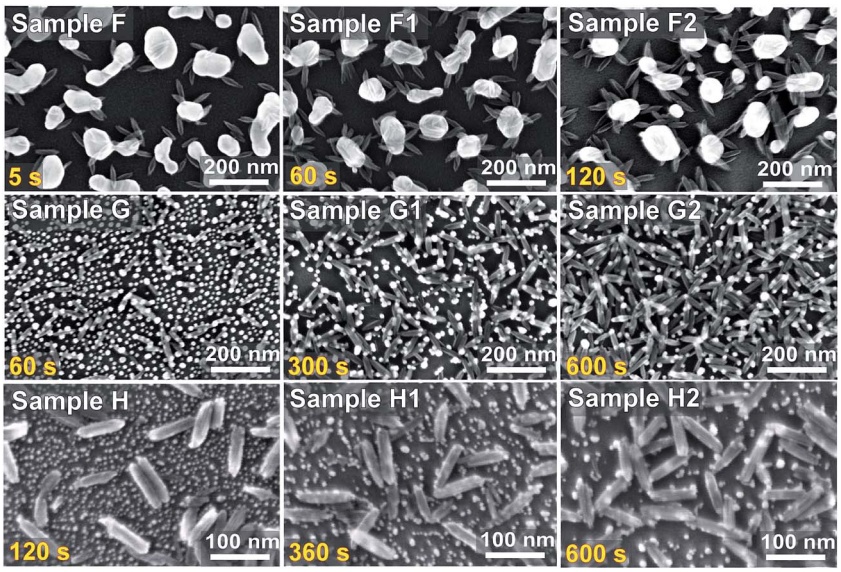

Fig. 2 SEM images of Fe nanorice particles electrodeposited at −1.0 V on bare Au nanoislands of different size ranges: (Sample F, F1 and F2) 50–200 nm, (Sample G, G1 and G2) 10–30 nm, and (Sample H, H1 and H2) 5–10 nm (note the change in scale), with increasing deposition time.

PDI-functionalized Au NI template (Fig. 1, Sample A1). In contrast, obvious aggregation of Au NIs is found for the bare or non-functionalized Au NI template (Fig. 1, Sample A2). This is believed to be due to field-induced relocation of Au nanoparticles smaller than 10 nm. However, such relocation and aggregation is not observed at an applied voltage of −1.0 V, indicating that the applied field is not strong enough to dislodge the Au nanoparticles. However, in our electrolyte solution containing 10 mM $FeCl_3$ and 100 mM $NaClO_4$, the morphologies of PDI-functionalized (Fig. 1, Sample B) and bare Au NI templates (Fig. 1, Sample C) become critically different even upon applying the potential of −1.0 V. This is likely due to the increase in ionic conductivity upon adding $FeCl_3$ and the $NaClO_4$ supporting electrolyte (when compared to the blank solution). Nonetheless, the PDI-functionalized Au NIs remain intact while the bare Au NIs rearrange to form bigger islands resulting in a decreased number density on the Si substrate. Sohn *et al.* also observed relocation of Au nanoparticles upon Pd electrodeposition on Au NI template.[48] This observation indicates that functionalization of Au is a very important step for fabricating Au-hybridized materials by electrochemistry. It is, however, not clear that whether Au relocation protection by PDI is due to enhanced conduction between Au NPs and Si surface resulting from oligomerization of PDI.[42,43]

The complementary case has also been examined by preparing Au on Fe NrPs by magnetron sputtering (Fig. 1, Sample D) and electrodeposition (Fig. 1, Sample E). As expected, the Au NIs are deposited uniformly on both Fe NrPs and the exposed parts of Si substrate not covered by the Fe NrPs by magnetron sputtering, but preferentially on Fe NrPs than Si by electrodeposition due to a higher local deposition on Fe than on Si. Comparison of their interfacial properties with those of Fe on Au NI template by using XPS is discussed below.

To examine the size effect of Au NIs, we electrochemically deposit Fe with increasing deposition time on Au NIs with different sizes ranging from 5 to 200 nm, shown in Fig. 2. For the larger bare Au NIs (~100 nm, Fig. 2, Sample F), the Au NIs are not affected by Fe deposition, and Fe NrPs are found to be preferentially deposited on top of the Au NIs and not directly on the exposed part of the Si support. As expected, the number of Fe NrPs near an Au NI increases with increasing deposition time (Fig. 2, Samples F1 and F2). This represents a modified way of preparing Fe–Au hybrid material by electrodeposition. For the smaller bare Au NIs of 10–30 nm in size, the number of Fe NrPs also increases with increasing deposition time (Fig. 2, Samples G, G1 and G2). Surprisingly, the Au NIs clearly undergo spatial reorganization on the substrate with increasing deposition time, as the Au NIs become more hybridized with the Fe NrPs, which gives the appearance that the Fe NrP surfaces are functionalized/decorated by Au NIs. For the even smaller Au NIs of 5–10 nm in size, aggregation to form bigger islands and hybridization with the Fe NrPs with increasing deposition time are also observed (Fig. 2, Samples H, H1 and H2). These changes are likely due to the effect of applied potential as discussed above. The number density of Au NIs has therefore drastically decreased with increasing deposition time. In contrast, the larger Au nanoparticles are found to be not aggregated (Fig. 2, Sample F). This is consistent with the applied potential being not strong enough to break the larger numbers of Au–Si bond to dislodge the bigger Au nanoparticles from the Si substrate. Other SEM images for Fe electrodeposition on a bare Si, bare and PDI-functionalized Au NI templates are provided in ESI, Fig. S2 and S3.†

Fig. 3 compares the XPS spectra of electrodeposited Fe NrPs on a PDI-functionalized Au NI template (Sample B) with those of on a bare Au NI template (Sample C). As these two sets of depth-profiling XPS spectra are found to be remarkably similar, they will be discussed together. For the as-prepared sample (*i.e.* before sputtering), the Fe $2p_{3/2}$ (Fe $2p_{1/2}$) peak located at 711.1 eV (724.8 eV, with a spin–orbit splitting of 13.7 eV) is

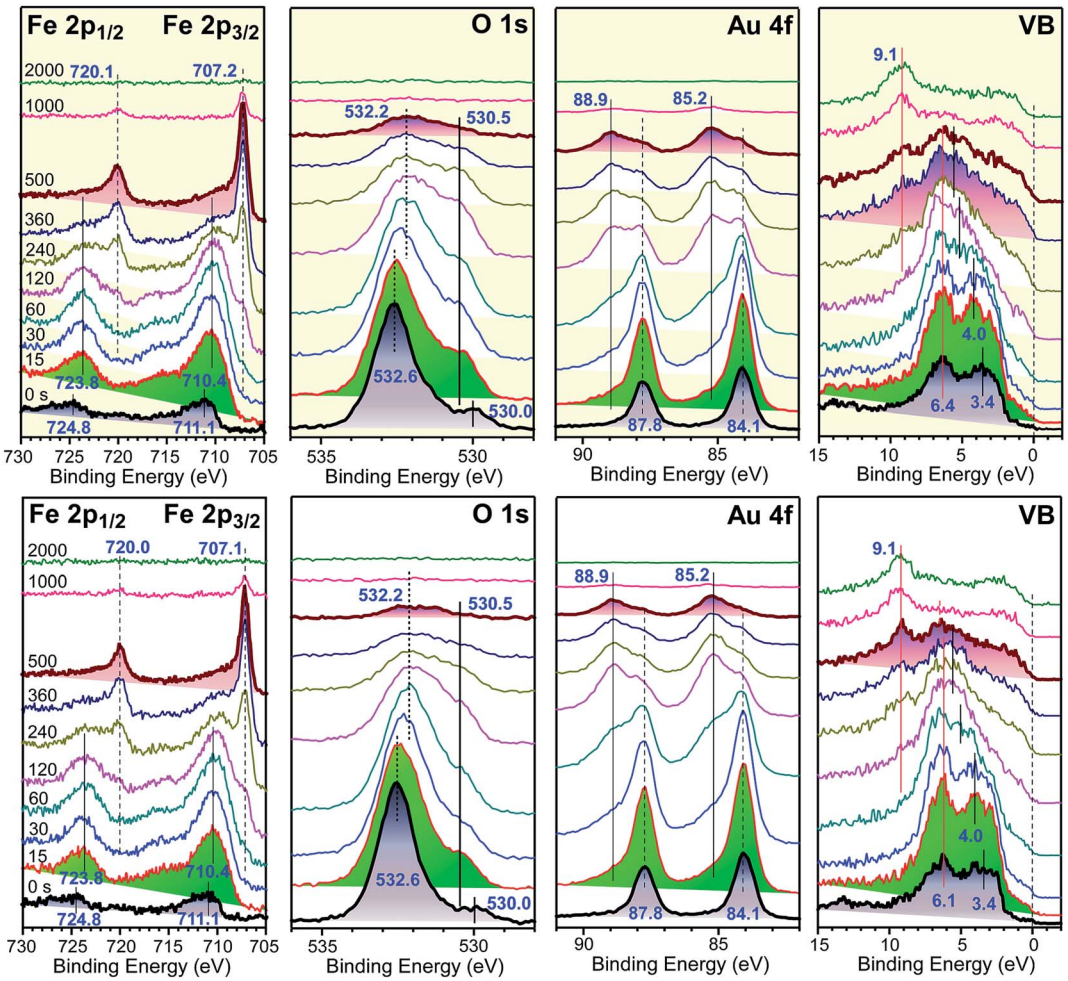

Fig. 3 XPS spectra of Fe 2p, O 1s, Au 4f and valence-band (VB) regions of Fe as-electrodeposited on Au nanoisland template with (top) and without (bottom) PDI functionalization, and with increasing Ar ion sputtering time to 2000 s.

attributable to Fe_2O_3 and/or FeOOH.[41] The corresponding O 1s feature appears as a weak feature at 530.0 eV, while the intense O 1s peak at 532.6 eV corresponds to the SiO_x support not covered by the Au NIs. The peak at 532.6 eV appears to shift slightly to 532.2 eV as the oxidation state of SiO_x changes upon sputtering. To assist with our assignment, we determine the relative Fe-to-O composition from the areas of the Fe 2p peaks and the O 1s feature at 530.0 eV, taking into account of their corresponding sensitivity factors (Fe 2p = 3.0 and O 1s = 0.66). The surface Fe-to-O composition is calculated to be $Fe_1O_{1.56}$, which is in good accord with our assignment of Fe_2O_3 or mixed FeO/FeOOH. The Au $4f_{7/2}$ (Au $4f_{5/2}$) peak at 84.1 eV (87.8 eV) corresponds to metallic Au. The valence band (VB) features also resemble mostly those of metallic Au,[47] indicating that they are dominated by Au NIs than Fe NrPs. Upon 15 s of sputtering, the Fe $2p_{3/2}$ (Fe $2p_{1/2}$) peak has shifted to 710.4 eV (723.8 eV), which could be attributable to either Fe_3O_4 or FeO, or both.[41,49] The spin–orbit splitting becomes 13.4 eV, and the calculated Fe-to-O ratio is 1 : 1.01, which supports the assignment of FeO. The FeO feature becomes gradually reduced upon further sputtering but remains detectable after 360 s sputtering. After 120 s sputtering, a new Fe $2p_{3/2}$ (Fe $2p_{1/2}$) peak at 707.2 eV (720.1 eV, with an observed spin–orbit splitting of 12.9 eV) emerges and can be attributed to the metallic Fe core of the Fe NrPs. Further sputtering for over 500 s effectively removes the Fe 2p and O 1s features attributed to FeO, while the Fe 2p peak of the metallic Fe becomes a major component. The metallic Fe 2p remains at the same binding energy location without discernible change with increasing sputtering time, indicating no quantum size effect or alloying (due to formation of Fe silicide) at the interface of metallic Fe and Si support.

The new broader Au $4f_{7/2}$ (Au $4f_{5/2}$) feature at 85.2 eV (88.9 eV) appears upon just 15 s sputtering and becomes more intense with increasing sputtering to 120 s. These features could be assigned to Au–Si alloy.[47] The intensities of both the metallic Au and the Au–Si peaks are diminished as the Au NIs are reduced with continued sputtering. Furthermore, the peak separation between the VB features at 6.4 eV and 3.4 eV is also found to become smaller with increasing sputtering time.[47] Finally, the remarkable similarity between the depth-profiling XPS spectra for Fe NrPs on Au NI templates with and without PDI functionalization indicates that PDI functionalization of the Au NIs does not introduce additional changes to the interfacial structures of Fe–Au. This suggests that Fe NrPs could be grown on

top of Au NIs without disturbing the Au NIs even in the presence of attached PDI. On the other hand, bare Au NPs are clearly hybridized by the presence of electrodeposited Fe NrPs.

The XPS spectra of the Fe NrPs selectively grown on bigger (50–200 nm) Au NIs (Sample F1) were also examined (ESI, Fig. S4†). For the as-prepared sample, the Fe $2p_{3/2}$ (Fe $2p_{1/2}$) peak at 711.3 eV (724.9 eV, with a spin–orbit splitting of 13.6 eV) is also in accord with their assignment to Fe_2O_3 or FeOOH, which is supported by their calculated Fe-to-O surface composition of 1 : 1.48. Upon a short sputtering of 30 s, the Fe $2p_{3/2}$ (Fe $2p_{1/2}$) and O 1s features are found to shift to 710.4 eV (723.4 eV) and 530.5 eV, respectively, indicating the emergence of FeO. Qualitatively, the Fe 2p, O 1s, Au 4f and VB spectra exhibit similar change with sputtering as the spectra for those Fe NrPs grown on smaller Au NIs, shown in Fig. 3.

It is of interest to compare the interfacial compositions of Fe NrPs electrodeposited on Au NIs (Fig. 1, Samples B and C) with Au either sputter-deposited (Fig. 1, Sample D) or electrodeposited (Fig. 1, Sample E) on a Fe NrP template. Because the latter two samples (Samples D and E) show very similar XPS spectra with sputtering depth, we only discuss comparison with the depth-profiling spectra of sputter-deposited Au on Fe NrP, shown in Fig. 4. Upon sputtering of 15 s, a broad weak Au $4f_{7/2}$ photoemission feature at 85.2 eV, appearing as a shoulder of the metallic peak at 84.1 eV, becomes detectable and more intense with increasing sputtering with no discernible binding energy shift. This higher Au $4f_{7/2}$ peak has been commonly attributed to Au silicide.[47] Upon sputtering more than 120 s, the metallic Au $4f_{7/2}$ peak is found to gradually shift to a higher binding energy with increasing sputtering time and the observed Au $4f_{7/2}$ peak shift becomes +0.7 eV for sputtering for 500 s. As the gradual Au 4f binding energy shift is not observed for the Fe NrP on Au NIs sample (Sample B and C in Fig. 3, and Sample F1 in ESI, Fig. S4†), such gradual shift for Sample D could be related to formation of a new cationic Au species involving, *e.g.*, Au–O bonding on the iron oxide surface. We rule out quantum size effect[50] here because for Samples B, C and F1 no gradual binding energy shift for Au 4f is observed for the Fe NrP on bare Au NI sample despite the reduction in the Au size with increasing sputtering time. In addition, the Fe $2p_{3/2}$ peak at 711.1 eV for the as-prepared Au on Fe NrP sample is found to be very weak, which indicates that the Fe NrPs are very much covered by Au. Upon 15 s of sputtering, the Fe peak corresponding to FeO becomes dominant and remains prominent until 1000 s sputtering. The O atoms of the topmost layer of Fe_2O_3 or FeOOH may indeed react with the deposited Au atoms, producing the Au–O bonding at the interface and the observed binding energy shift in Au 4f peak.

The chemical state of Au generally depends upon the preparation method and thermal treatment.[51–57] For Au supported on Fe_2O_3 prepared by a co-precipitation method, Visco *et al.* concluded, on the basis of XPS data, that both metallic and oxidized Au (Au–O) species are present on the surface of the samples.[49] They also observed an increase in the intensity of the metallic Au feature upon a higher temperature reaction. Hutchings *et al.* also found a very similar result for Au on Fe oxides prepared by a co-precipitation method.[57] For Au prepared by a deposition-precipitation method, Khoudiakov *et al.* found a mixed metallic (major) and cationic (minor) Au species in their Au 4f XPS study.[56] Metallic Au 4f peak has also commonly been found for Au on Fe oxides prepared by co-precipitation, deposition-precipitation and reduction methods,[51,52,54,55,58] with a lower binding energy than that reported for bulk Au.[51,55,58] This latter negative binding energy shift has been attributed to a support effect arising from metal-support charge transfer interaction.[19,58] We summarize the literature reports on the binding energy positions of different Au species in Table S1 (ESI†).

Finally, Fig. 5 summarizes schematically the nature and the variety of the Fe–Au hybrid materials obtained in the present work. For Fe NrPs electrodeposited on a PDI-functionalized Au NI template (Fig. 5, Sample B), Fe deposition do not disturb the Au NIs, which appear to be well protected by the PDI overlayer. This sample of Fe NrPs on Au NIs is quite different from the

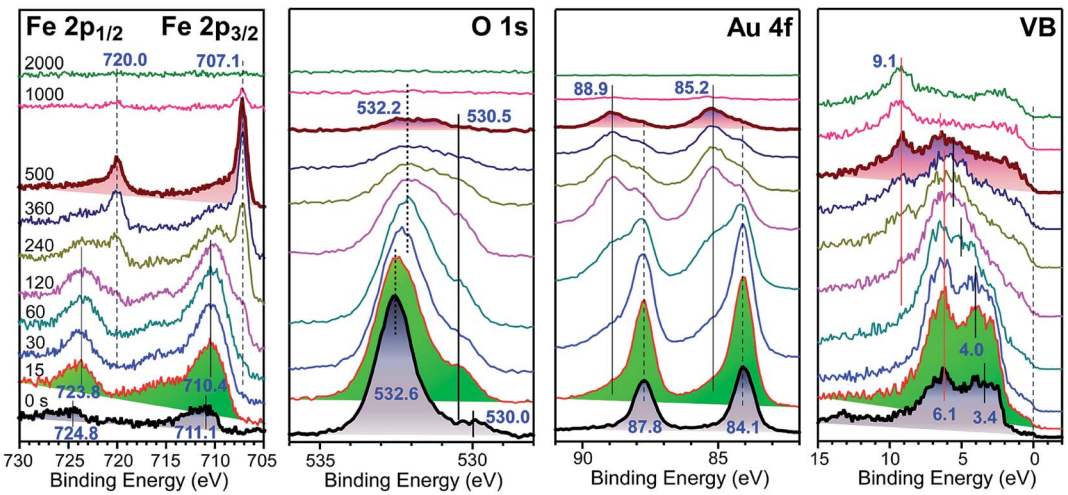

Fig. 4 XPS spectra of Fe 2p, O 1s, Au 4f and valance-band (VB) regions of Au sputter-deposited on a Fe NrP template (shown in Fig. 1, Sample D), as-prepared and with sputtering to 2000 s.

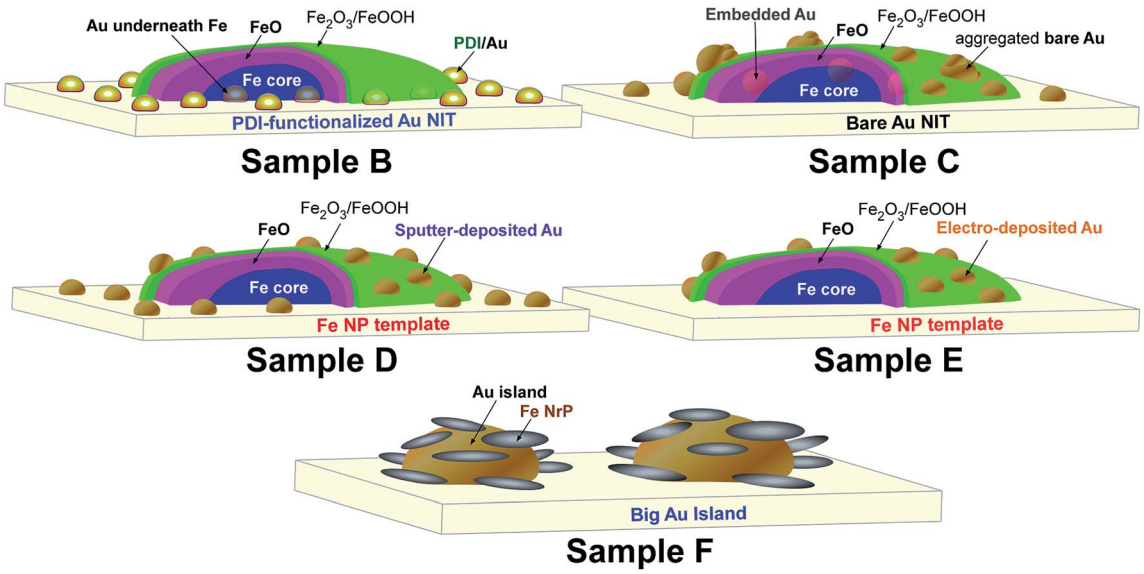

Fig. 5 Schematic models of Fe electrodeposited on PDI-functionalized (Fig. 1, Sample B) and bare Au nanoisland templates (NITs) (Fig. 1, Sample C), and of Au deposited on Fe nanorice particle (NrP) template by magnetron sputtering (Fig. 1, Sample D) and by electrodeposition (Fig. 1, Sample E), and of preferential Fe deposition on larger Au islands (Fig. 2, Sample F).

sample of Fe NrPs electrodeposited on a bare Au NI template without PDI functionalization (Fig. 5, Sample C), where the Au NIs hybridize with the Fe NrPs, with coverage on top and embedment inside, and with some Au NIs aggregating to form a bigger island. For Au sputter-deposited on a Fe NrP template (Fig. 5, Sample D), Au is deposited on both the surface of Si substrate and Fe NrP (but with no evidence for aggregation and embedment). For Au electrodeposited on a Fe NrP template (Fig. 5, Sample E), Au is predominantly deposited on the surface of Fe NrP due to the more favourable conductivity. Both of these produce the third type of hybrid materials, with Fe NrP coated by Au NIs. In addition, Fe is also preferentially electrodeposited on a large Au NI, producing a Fe NrP coated form of Au–Fe hybrid material (Fig. 5, Sample F).

4. Conclusions

PDI functionalization has been shown to protect and anchor down Au NIs on Si during Fe electrochemical deposition. In other words, Fe NrPs could be electrodeposited on Au NI templates without impacting the Au NI templates. Without PDI functionalization, the Au NIs are easily disturbed by the applied electrodeposition potential and become hybridized with the Fe NrPs. On the basis of the XPS results, we conclude that the electrodeposited Fe NrP consists of a metallic Fe-core with a FeO shell covered by a thin outermost Fe_2O_3/FeOOH skin. No detectable new species (*e.g.*, Fe–Au interfacial alloy or Au–O containing species) is found at the interface. For Au electrodeposited (or sputter-deposited) on top of Fe NrP, a new cationic Au species involving the formation of Au–O bonding is found at the interface. We also show that Fe NrPs could be preferentially electrodeposited on larger Au NIs to produce a new-type nano-hybrid material using a modified deposition method. The present work therefore demonstrates the formation of a variety of novel nano-on-nano hybrid materials with and without the use of PDI functionalization before electrochemical deposition.

Acknowledgements

This work was supported by the Natural Sciences and Engineering Research Council of Canada.

Notes and references

1 J. B. Sambur and P. Chen, *Annu. Rev. Phys. Chem.*, 2014, **65**, 395–422.
2 Z.-C. Zhang, B. Xu and X. Wang, *Chem. Soc. Rev.*, 2014, **43**, 7870–7886.
3 L. Jiang and Z. Fan, *Nanoscale*, 2014, **6**, 1922–1945.
4 J. Jiang, Y. Li, J. Liu, X. Huang, C. Yuan and X. W. Lou, *Adv. Mater.*, 2012, **24**, 5166–5180.
5 T. Salim, S. Sun, Y. Abe, A. Krishna, A. C. Grimsdale and Y. M. Lam, *J. Mater Chem. A*, 2015, DOI: 10.1039/c4ta05226a.
6 J. Tang, J. Liuc, N. L. Torad, T. Kimurad and Y. Yamauchi, *Nano Today*, 2014, **9**, 305–323.
7 M. C. Orilall and U. Wiesner, *Chem. Soc. Rev.*, 2011, **40**, 520–535.
8 H. Cheng, B. Huang and Y. Dai, *Nanoscale*, 2014, **6**, 2009–2026.
9 M. D. Susman, Y. Feldman, A. Vaskevich and I. Rubinstein, *ACS Nano*, 2014, **8**, 162–174.
10 Y. Bai, W. Zhang, Z. Zhang, J. Zhou, X. Wang, C. Wang, W. Huang, J. Jiang and Y. Xiong, *J. Am. Chem. Soc.*, 2014, **136**, 14650–14653.
11 C. J. Zhong and M. M. Maye, *Adv. Mater.*, 2001, **13**, 1507–1511.
12 Q. Li, Y. Yuan, Z. Chen, X. Jin, T.-H. Wei, Y. Li, Y. Qin and W. Sun, *ACS Appl. Mater. Interfaces*, 2014, **6**, 12798–12807.

13 R. Ferrando, J. Jellinek and R. L. Johnston, *Chem. Rev.*, 2008, **108**, 845–910.
14 X. Peng, Q. Pan and G. L. Rempel, *Chem. Soc. Rev.*, 2008, **37**, 1619–1628.
15 H. J. Freund and G. Pacchioni, *Chem. Soc. Rev.*, 2008, **37**, 2224–2242.
16 D. Widmann and R. J. Behm, *Acc. Chem. Res.*, 2014, **47**, 740–749.
17 Z. P. Liu, S. J. Jenkins and D. A. King, *Phys. Rev. Lett.*, 2005, **94**, 196102/1–196102/4.
18 J. Saavedra, H. A. Doan, C. J. Pursell, L. C. Grabow and B. D. Chandler, *Science*, 2014, **345**, 1599–1602.
19 M. Haruta, *Angew. Chem., Int. Ed.*, 2014, **53**, 52–56.
20 G. C. Bond and D. T. Thompson, *Catal. Rev.: Sci. Eng.*, 1999, **41**, 319–388.
21 A. S. K. Hashmi and G. J. Hutchings, *Angew. Chem., Int. Ed.*, 2006, **45**, 7896–7936.
22 S. Eustis and M. A. El-Sayed, *Chem. Soc. Rev.*, 2006, **35**, 209–217.
23 S. Laurent, D. Forge, M. Port, A. Roch, C. Robic, L. V. Elst and R. N. Muller, *Chem. Rev.*, 2008, **108**, 2064–2110.
24 J. Gallo, N. Kamaly, I. Lavdas, E. Stevens, Q.-D. Nguyen, M. Wylezinska-Arridge, E. O. Aboagye and N. J. Long, *Angew. Chem., Int. Ed.*, 2014, **53**, 9550–9554.
25 A. Gonzalez-de-Castro, C. M. Robertson and J. Xiao, *J. Am. Chem. Soc.*, 2014, **136**, 8350–8360.
26 L. Machala, R. Zboril and A. Gedanken, *J. Phys. Chem. B*, 2007, **111**, 4003–4018.
27 N. A. Hodge, C. J. Kiely, R. Whyman, M. R. H. Siddiqui, G. J. Hutchings, Q. A. Pankhurst, F. E. Wagner, R. R. Rajaramand and S. E. Golunski, *Catal. Today*, 2002, **72**, 133–144.
28 M. Khoudiakov, M. C. Gupta and S. Deevi, *Nanotechnology*, 2004, **15**, 987–990.
29 W. Deng, C. Carpenter, N. Yi and M. Flytzani-Stephanopoulos, *Top. Catal.*, 2007, **44**, 199–208.
30 R. M. Finch, N. A. Hodge, G. J. Hutchings, A. Meagher, Q. A. Pankhurst, M. R. H. Siddiqui, F. E. Wagner and R. Whyman, *Phys. Chem. Chem. Phys.*, 1999, **1**, 485–489.
31 N. M. Gupta and A. K. Tripathi, *Gold Bull.*, 2001, **34**, 120–128.
32 M. Haruta and M. Date, *Appl. Catal., A*, 2001, **222**, 427–437.
33 W. Gu, X. Deng, X. Gu, X. Jia, B. Lou, X. Zhang, J. Li and E. Wang, *Anal. Chem.*, 2015, **87**, 1876–1881.
34 J. Bao, W. Chen, T. Liu, Y. Zhu, P. Jin, L. Wang, J. Liu, Y. Wei and Y. Li, *ACS Nano*, 2007, **1**, 293–298.
35 W. P. Li, P. Y. Liao, C. H. Su and C. S. Yeh, *J. Am. Chem. Soc.*, 2014, **136**, 10062–10075.
36 C. G. Wang, J. J. Chen, T. Talavage and J. Irudayaraj, *Angew. Chem., Int. Ed.*, 2009, **48**, 2759–2763.
37 C. J. Xu, B. D. Wang and S. H. Sun, *J. Am. Chem. Soc.*, 2009, **131**, 4216–4217.
38 Z. Xu, Y. Hou and S. Sun, *J. Am. Chem. Soc.*, 2007, **129**, 8698–8699.
39 H. Wang, D. W. Brandl, F. Le, P. Nordlander and N. J. Halas, *Nano Lett.*, 2006, **6**, 827–832.
40 L. Y. Zhao, K. R. Eldridge, T. Chan, N. Panjwani and K. T. Leung, *Nanotechnology*, 2007, **18**, 245703–245708.
41 L. Y. Zhao, K. R. Eldridge, K. Sukhija, H. Jalili, N. F. Heinig and K. T. Leung, *Appl. Phys. Lett.*, 2006, **88**, 033111/1–033111/3.
42 J. Kestell, R. Abuflaha, J. A. Boscoboinik, Y. Bai, D. W. Bennett and W. T. Tysoe, *Chem. Commun.*, 2013, **49**, 1422–1424.
43 M. Garvey, J. Kestell, R. Abuflaha, D. W. Bennett, G. Henkelman and W. T. Tysoe, *J. Phys. Chem. C*, 2014, **118**, 20899–20907.
44 E. Lopez-Tobar, K. Hara, I. Izquierdo-Lorenzo and S. Sanchez-Cortes, *J. Phys. Chem. C*, 2015, **119**, 599–609.
45 Y. Sohn, D. Pradhan, L. Zhao and K. T. Leung, *Electrochem. Solid-State Lett.*, 2012, **15**, K35–K39.
46 Y. Sohn and J. M. White, *J. Phys. Chem. C*, 2008, **112**, 5006–5013.
47 Y. Sohn, D. Pradhan, A. Radi and K. T. Leung, *Langmuir*, 2009, **25**, 9557–9563.
48 Y. Sohn, D. Pradhan and K. T. Leung, *ACS Nano*, 2010, **4**, 5111–5120.
49 A. M. Visco, F. Neri, G. Neri, A. Donato, C. Milone and S. Galvagno, *Phys. Chem. Chem. Phys.*, 1999, **1**, 2869–2873.
50 H. G. Boyen, A. Ethirajan, G. Kästle, F. Weigl, P. Ziemann, G. Schmid, M. G. Garnier, M. Büttner and P. Oelhafen, *Phys. Rev. Lett.*, 2005, **94**, 016804/1–016804/4.
51 D. Horvath, L. Toth and L. Guczi, *Catal. Lett.*, 2000, **67**, 117–128.
52 H. Y. Lin and Y.-W. Chen, *Ind. Eng. Chem. Res.*, 2005, **44**, 4569–4576.
53 A. P. Kozlova, A. I. Kozlov, S. Sugiyama, Y. Matsui, K. Asakura and Y. Iwasawa, *J. Catal.*, 1999, **181**, 37–48.
54 L. Wang, J. Luo, Q. Fan, M. Suzuki, I. S. Suzuki, M. H. Engelhard, Y. Lin, N. Kim, J. Q. Wang and C.-J. Zhong, *J. Phys. Chem. B*, 2005, **109**, 21593–21601.
55 Z. Zhong, J. Ho, J. Teo, S. Shen and A. Gedanken, *Chem. Mater.*, 2007, **19**, 4776–4782.
56 M. Khoudiakov, M. C. Gupa and S. Deevi, *Appl. Catal., A*, 2005, **291**, 151–161.
57 G. J. Hutchings, M. S. Hall, A. F. Carley, P. Landon, B. E. Solsona, C. J. Kiely, A. Herzing, M. Makkee, J. A. Moulijn, A. Overweg, J. C. Fierro-Gonzalez, J. Guman and B. C. Gates, *J. Catal.*, 2006, **242**, 71–81.
58 S. Arrii, F. Morfin, A. J. Renouprez and J. L. Rousset, *J. Am. Chem. Soc.*, 2004, **126**, 1199–1205.